PFG (2022) 90:177–189
https://doi.org/10.1007/s41064-021-00189-2

ORIGINAL ARTICLE

Modeling Secchi Disk Depth Over the North Arabian Gulf Waters Using MODIS and MERIS Images

Mohammad M. M. Alsahli[1,2] · **Majid Nazeer**[3]

Received: 27 November 2020 / Accepted: 20 December 2021 / Published online: 31 January 2022

Abstract

Water transparency measured using Secchi disk is an important water quality indicator influenced by various biotic and abiotic processes in coastal and marine ecosystems. Understanding the role of this important indicator over large coastal environments requires synoptic measurements through ocean color satellites, such as Moderate-Resolution Imaging Spectroradiometer (MODIS) and Medium-Resolution Imaging Spectrometer (MERIS). In this study, we evaluated the performance of different atmospheric correction algorithms and the suitability of different pixel extraction methods in modeling Secchi disk depth (Z_{SD}) over the North Arabian Gulf (NAG) waters using MODIS and MERIS imagery. Evaluating the performance of different atmospheric correction algorithms and the suitability of pixel extraction methods yielded various Z_{SD} models with different accuracy. The most accurate MODIS and MERIS Z_{SD} models had R^2 of 0.75 (RMSE = 80 cm) and 0.78 (RMSE = 74 cm), respectively. These models can be used to accurately map Z_{SD} of NAG waters that would provide a better understanding of NAG water quality dynamics. Although these models were designed for NAG waters, they can be applied for the entire Arabian Gulf waters and probably other similar waters with the availability of training data. The key factor that limits the efficiency of these models and other previous models is the success of atmospheric correction algorithms in retrieving reliable remote sensing reflectance over different water bodies.

Keywords Water quality · Remote sensing modeling · Coastal environment · Ocean color satellite images · Water clarity · Kuwait Bay

✉ Mohammad M. M. Alsahli
m.alsahli@ku.edu.kw

Majid Nazeer
majid.nazeer@connect.polyu.hk

[1] Department of Geography, College of Social Sciences, Kuwait University, Safat, P.O. Box 5969, 13060 Kuwait City, Kuwait

[2] GIS and Remote Sensing Consultation Unit, College of Social Sciences, Kuwait University, Safat, P.O. Box 5969, 13060 Kuwait City, Kuwait

[3] School of Geography and Environment, Jiangxi Normal University, Nanchang 330022, Jiangxi, China

Zusammenfassung

Modellierung der Secchi-Scheibentiefe über den Gewässern des Nordarabischen Golfs mit MODIS- und MERIS-Bildern. Die mit der Secchi-Scheibe gemessene Wassertransparenz ist ein wichtiger Indikator für die Wasserqualität, der durch verschiedene biotische und abiotische Prozesse in Küsten- und Meeresökosystemen beeinflusst wird. Um die Rolle dieses wichtigen Indikators in großen Küstenumgebungen zu verstehen, sind synoptische Messungen durch Ozeanfarbsatelliten wie das Moderate-Resolution Imaging Spectroradiometer (MODIS) und das Medium-Resolution Imaging Spectrometer (MERIS) erforderlich. In dieser Studie bewerteten wir die Leistung verschiedener atmosphärischer Korrekturalgorithmen und die Eignung verschiedener Pixelextraktionsmethoden bei der Modellierung der Secchi-Scheibentiefe (Z_{SD}) über den Gewässern des Nordarabischen Golfs (NAG) unter Verwendung von MODIS- und MERIS-Bildern. Die Bewertung der Leistung verschiedener atmosphärischer Korrekturalgorithmen und der Eignung von Pixelextraktionsmethoden ergab verschiedene Z_{SD}-Modelle mit unterschiedlicher Genauigkeit. Die genauesten MODIS- und MERIS Z_{SD}-Modelle erreichten R^2 von 0,75 (RMSE = 80 cm) bzw. 0,78 (RMSE = 74 cm). Diese Modelle können verwendet werden, um Z_{SD} von NAG-Gewässern genau abzubilden, was ein besseres Verständnis der NAG-Wasserqualitätsdynamik ermöglichen würde. Obwohl diese Modelle für NAG-Gewässer entwickelt wurden, können sie für die gesamten Gewässer des Arabischen Golfs und wahrscheinlich andere ähnliche Gewässer bei der Verfügbarkeit von Trainingsdaten angewendet werden. Der Schlüsselfaktor, der die Effizienz dieser Modelle und anderer früherer Modelle einschränkt, ist der Erfolg atmosphärischer Korrekturalgorithmen bei der Gewinnung zuverlässiger Fernerkundungsreflexion über verschiedene Gewässer.

1 Introduction

Water transparency is a crucial factor for understanding the status of the aquatic ecosystem. It controls the amount of light available for autotrophs occupying the first layer in the aquatic food chain. Water transparency is influenced by other important water quality variables [i.e., chlorophyll-*a* concentrations (Chl-*a*), colored dissolved organic matter (CDOM) and total suspended sediments (TSS)] (Chang et al. 2013; Song et al. 2014; Alikas and Kratzer 2017). These water constituents are linked to biotic and abiotic processes in coastal and marine ecosystems, including phytoplankton abundance, bacterial activity and interrelationships between inland waters and coastal ecosystems (Kaiser et al. 2011; Cherukuru et al. 2014; Boufeniza et al. 2020). Thus, synoptic monitoring of water transparency is fundamental to understanding, maintaining, and sustaining coastal and marine ecosystems.

Water transparency has been routinely monitored for decades by measuring the depth of Secchi disk (Z_{SD}), a white or white and black disk with 20–30 cm diameter (Preisendorfer 1986; Lewis et al. 1988; Liu et al. 2019). Due to the simple procedure for estimating Z_{SD}, large datasets of in situ Z_{SD} have been established for many sites worldwide (Seafarers et al. 2017). However, such in situ data cannot efficiently represent the water transparency of coastal and marine areas in a spatial–temporal context. Mapping spatial and temporal distributions of Z_{SD} requires an integrated approach that incorporates in situ data and ocean color images, such as those from Moderate-Resolution Imaging Spectroradiometer (MODIS) and Medium-Resolution Imaging Spectrometer (MERIS).

Various approaches were used to map Z_{SD} in different aquatic ecosystems using remotely sensed data. The accuracy of these approaches was influenced by multiple factors, including the selection of atmospheric correction algorithm, modeling method and in situ-remotely sensed data matching criteria and time window (e.g., Constantin et al. 2016; Kulshreshtha and Shanmugam 2017). A standard approach of atmospheric correction assumes negligible reflectance from near-infrared (NIR) bands over water bodies. This approach is successfully used to estimate Z_{SD} in open seas and oceans where Chl-*a* concentrations mainly control the optical properties of waters (e.g., Lewis et al. 1988; Seafarers et al. 2017; Shi et al. 2014). However, this standard atmospheric correction approach is less efficient in turbid waters where the reflectance from NIR bands cannot be ignored (Hu et al. 2000; Wang et al. 2012).

Two alternative atmospheric correction approaches were developed to improve the reliability of remote sensing reflectance (Rrs) over turbid waters, i.e., Management Unit of the North Sea Mathematical Models (MUMM) atmospheric correction algorithm developed by Ruddick et al. (2006) and Near Infrared-Short Wave Infrared (NIR-SWIR) atmospheric algorithm developed by Shi and Wang (2007). The MUMM atmospheric algorithm justifies Rrs at NIR wavelengths by a parameter derived by ratioing two Rrs of NIR bands. The algorithm also derives the aerosol reflectance over clear waters and applies it to the image, assuming that the atmospheric composition is relatively homogeneous over the area of interest. The NIR-SWIR atmospheric algorithm corrects Rrs over coastal waters utilizing SWIR bands, which are highly absorbed by turbid waters compared to NIR bands (Wang et al. 2009).

Furthermore, two modeling approaches (i.e., empirical and semi-analytical) can be used to derive Z_{SD}. Empirical models derive Z_{SD} statistically by comparing Rrs to simultaneous in situ Z_{SD} observations. The models are constructed either using simple regression analysis by regressing the product of the band ratio to in situ Z_{SD} or by using Rrs in different bands as predictors of Z_{SD} through multiple regression analysis or neural network analysis (Chen et al. 2015; Stock 2015; Kulshreshtha and Shanmugam 2017; Shi et al. 2018). Empirical models were usually constructed to map local or regional distributions of Z_{SD} (e.g., Toming et al. 2017; Zhang et al. 2012). Semi-analytical models resolve the apparent optical properties (AOP) using semi-analytically derived inherent optical properties (i.e., absorption, scattering and backscattering coefficients) based on the radiation transfer equation. Semi-analytical approaches attempted to propose a universal Z_{SD} model for both clear and turbid waters. Although the recent semi-analytical techniques provided a promising result in this matter (Lee et al. 2015; Shang et al. 2016), they still have lower performance over turbid waters than over clear waters (Liu et al. 2019). Thus, empirically deriving Z_{SD} using advanced statistical methods is still favorable for local and regional estimation of Z_{SD} (Kulshreshtha and Shanmugam 2017).

The accuracy of modeling Z_{SD} is also influenced by the time window used for matching Rrs with in situ data. Using a narrow time window between the satellite overpass and in situ measurements would reduce errors induced by temporal changes of water constituents (Bailey and Werdell 2006; Petus et al. 2014). Another potential source of errors is the way of matching in situ measurements with satellite data. In situ measurements are usually compared to a group of pixels, i.e., 3×3, 5×5 or 7×7 pixels, centered at each in situ point to overcome the positional uncertainty introduced by satellite images (Bailey and Werdell 2006). These pixel values are more frequently aggregated by the mean value that can be misleading when presenting a group of heterogeneous pixels. To reduce the effect of heterogeneity on the mean value, Bailey and Werdell (2006) excluded outlier pixels that exceed predefined lower and upper-value limits. Also, they stated that using a larger group of pixels would increase the heterogeneity effect, especially in dynamic waters. To overcome the heterogeneity issue, Chen et al. (2007) suggested excluding the mean value of matching pixels when its coefficient of variation (CV) is greater than 40%. Another remedy of the heterogeneity effect is to use the median value, which is not affected by outliers (Goyens et al. 2013).

Systematic procedures of matching in situ Z_{SD} with satellite images and selecting the appropriate atmospheric correction algorithm and modeling technique are significant in constructing an accurate and robust model for Z_{SD} estimation. In the Northern Arabian (Persian) Gulf (NAG), there have been few attempts to model ZSD. Two Z_{SD} models derived from MODIS were established for the Arabian Gulf region by Alsahli (2009) and Al-Kaabi et al. (2016); both studies used the standard atmospheric algorithm. And, to our knowledge, Z_{SD} models derived from MERIS have not

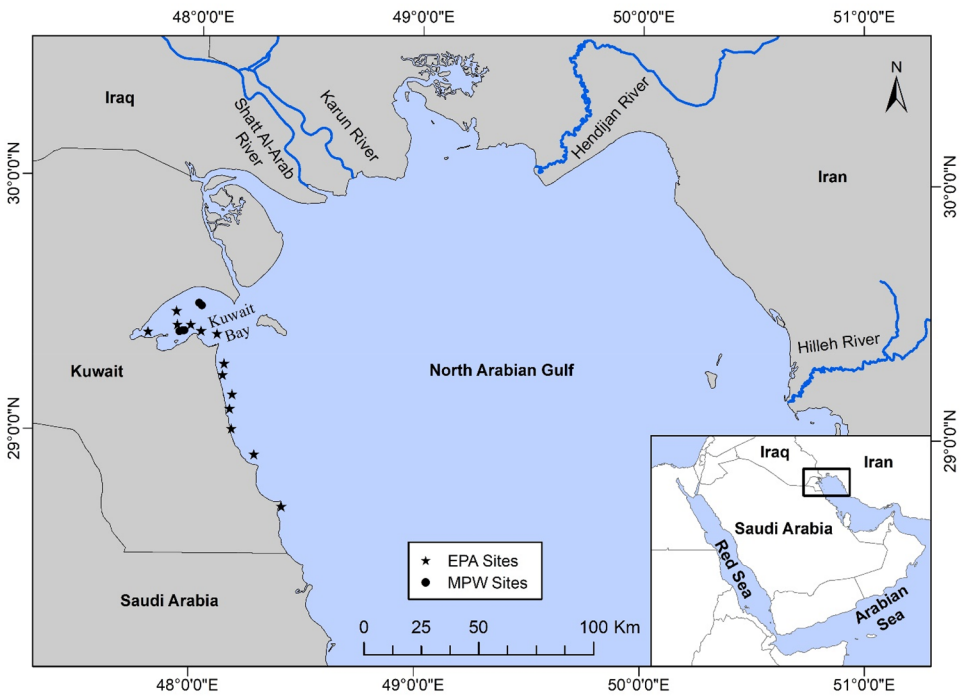

Fig. 1 The northern part of Arabian Gulf (NAG). The stars and black circles along Kuwait's territorial waters represent sites where seawater quality is observed by Kuwait Environmental Public Authority (KEPA) and Ministry of Public Works (MPW), respectively

been established yet for NAG waters. Therefore, this study aimed to: (1) examine the performance of three atmospheric correction algorithms (standard, MUMM and NIR-SWIR) over NAG, and (2) find the most optimum in situ-satellite image matching technique to construct an empirical model of Z_{SD} over NAG by investigating the relationship between in situ Z_{SD} and Rrs of MODIS and MERIS.

2 Study Area

The NAG lies within the geographic coordinates of 28° 31′ to 30° 01′ N and 47° 41′ to 51° 05′ E (Fig. 1). This part of the Arabian Gulf is shallow with less than 30 m in most areas, while the depth gradually increases towards the south. The general water movements in the NAG are governed by counter-clockwise circulations derived by the wind regime of the area (Al-Yamani et al. 2004). This circulation system enhances water transportation most of the year, from the eastern and northern banks of NAG to the western bank (Abuzinada et al. 2008). Freshwaters discharge into the NAG through five rivers, i.e., the Shatt Al-Arab, Karun, Hendijan, Hilleh, and Mond (also known as Mand in literature). The extensive anthropogenic activities along these rivers have degraded the water quality of the rivers and consequently contributed to changing NAG water characteristics, including the water transparency (Marzouni et al. 2014; Rahmanpour et al. 2014; Al-Mahmood and Mahmood 2019; Cunningham et al. 2019). Recently, Alsahli and Nazeer (2021) reported observable changes in the NAG water transparency during the last two decades. The NAG water transparency has been affected by regional and local factors, including dust storms and extensive anthropogenic activities along the NAG coasts (Al-Ghadban and El-Sammak 2005; Karbassi et al. 2005). Ultimately, this adds more environmental stress to the marine life of NAG (Alsahli 2009).

3 Data Used

3.1 In Situ Data

The in situ Z_{SD} data collected from Jan. 2003 to Apr. 2015 were used to model the water transparency using MODIS and MERIS images. This period was selected to maximize the number of in situ observations for model development and capture any potential seasonal variability affecting the model robustness. The in situ data were obtained from the Kuwait Environmental Public Authority (KEPA) and Ministry of Public Works (MPW) of Kuwait. The KEPA collects water quality data monthly at 13 sites along Kuwait territorial waters (Fig. 1). The MPW started collecting water quality data in 2013 to monitor the environmental status of Kuwait Bay during the Sheikh Jaber Al Ahmad Al Sabah Causeway Project, one of the mega projects in the country. In situ Z_{SD} data of MPW used in this study were collected in Kuwait Bay from Jul. 2013 to Apr. 2015 at six sites (Fig. 1). In situ Z_{SD} from both datasets (KEPA and MPW) ranged from 0.5 to 9.5 m.

3.2 Satellite Data

MODIS (Aqua) and MERIS data were used to model Z_{SD} over the NAG. MODIS and MERIS have almost a daily coverage of the study area, allowing finding more coincident in situ measurements with these satellite data. The MODIS sensors aboard Terra and Aqua platforms were launched during Dec. 1999 and May 2002, respectively. They cover the entire Earth's surface in 1–2 days with spatial resolutions ranging from 250 to 1000 m and an image swath width of 2330 km. MODIS Terra and Aqua overpass the study area approximately at 10:30 A.M. and 1:00 P.M. (local time), respectively. Both have identical multispectral bands suitable to observe bio-optical and physical characteristics of water bodies. MODIS Terra, however, has been experiencing a general system degradation since 2007, reducing its adequacy for quantitative analyses (Franz et al. 2008). Therefore, only MODIS Aqua level-1A data coincident with in situ data were obtained from the Ocean Color website (http://oceancolor.gsfc.nasa.gov).

Also, MERIS level-1 data coincident with in situ data were obtained from the Envisat MERIS website (http://merisfrs-merci-ds.eo.esa.int/merci). The MERIS images have a 300 m spatial resolution and have been collected for the study area around 10:00 A.M. (local time). The satellite mission was terminated in 2012 (Nilson et al. 2012). However, European Space Agency (ESA) continued MERIS mission by launching ESA Sentinel-3A and 3B during Feb. 2016 and Apr. 2018, respectively (Nilson et al. 2012; European Space Agency (ESA) 2018). The MERIS and current ESA satellites provide an important archive for studying biophysical variables of marine and coastal waters.

4 Methodology

4.1 Satellite Data Processing

MODIS and MERIS Images with wide viewing angles or affected by environmental conditions, such as dust storms and clouds, were disregarded to minimize potential errors when modeling Z_{SD} (Bailey and Werdell 2006). Also, $a \pm 3$-h window around the satellite overpass was selected for matching in situ observations with MODIS and MERIS data to reduce the differences due to the time factor between the two

datasets (Vaičiūtė et al. 2012). Alsahli (2009) revealed that using $a \pm 3$-h window around the satellite overpass was significantly reduced potential errors induced by the temporal variability in the in situ measurements. This time window has also been frequently used in other studies (e.g., Chen et al. 2014a, b; Delgado et al. 2014).

Selected MODIS and MERIS level-1 data were processed to level-2 using SeaWiFS Data Analysis System (SeaDAS 7.5) software. The MODIS level-1 data were processed to level-2 using three atmospheric algorithms (standard, MUMM and NIR-SWIR) to investigate their efficiency in minimizing effects of atmospheric perturbations over the study area, whereas the MERIS level-1 data were processed to level-2 using the standard atmospheric algorithm. When processing level-1 data to level-2, Rrs and normalized water-leaving radiance (nLw) (from 413 to 754 nm) were computed. The products of Rrs and nLw at these spectral bands have been frequently used in literature to estimate coastal water constituents, such as Z_{SD}, turbidity and TSS (e.g., Doron et al. 2011; Nechad et al. 2010; Stock 2015).

4.2 Satellite Data Extraction Criteria

The MODIS and MERIS level-2 data were matched with in situ data by extracting pixel values using a 3×3 window centered at each in situ point. The MODIS level-2 data consisted of three datasets processed based on three atmospheric algorithms (standard, MUMM and NIR-SWIR). To reduce the effect of pixels' heterogeneity, we investigated the suitability of four aggregation measures in matching the Rrs data with in situ Z_{SD} measurements. The mean value with CV $\leq 30\%$ (thereafter M-30), mean value with CV $\leq 15\%$ (thereafter M-15), median, and the filtered mean suggested by Bailey and Werdell (Bailey and Werdell 2006) (Eq. 1).

$$\text{Filtered mean} = \frac{\sum_i \left(1.5 \times \sigma - \overline{X}\right) < X_i < \left(1.5 \times \sigma + \overline{X}\right)}{n} \quad (1)$$

where $\overline{X}$ and σ are the mean and standard deviation, respectively, of the extracted pixel values at each in situ point, and

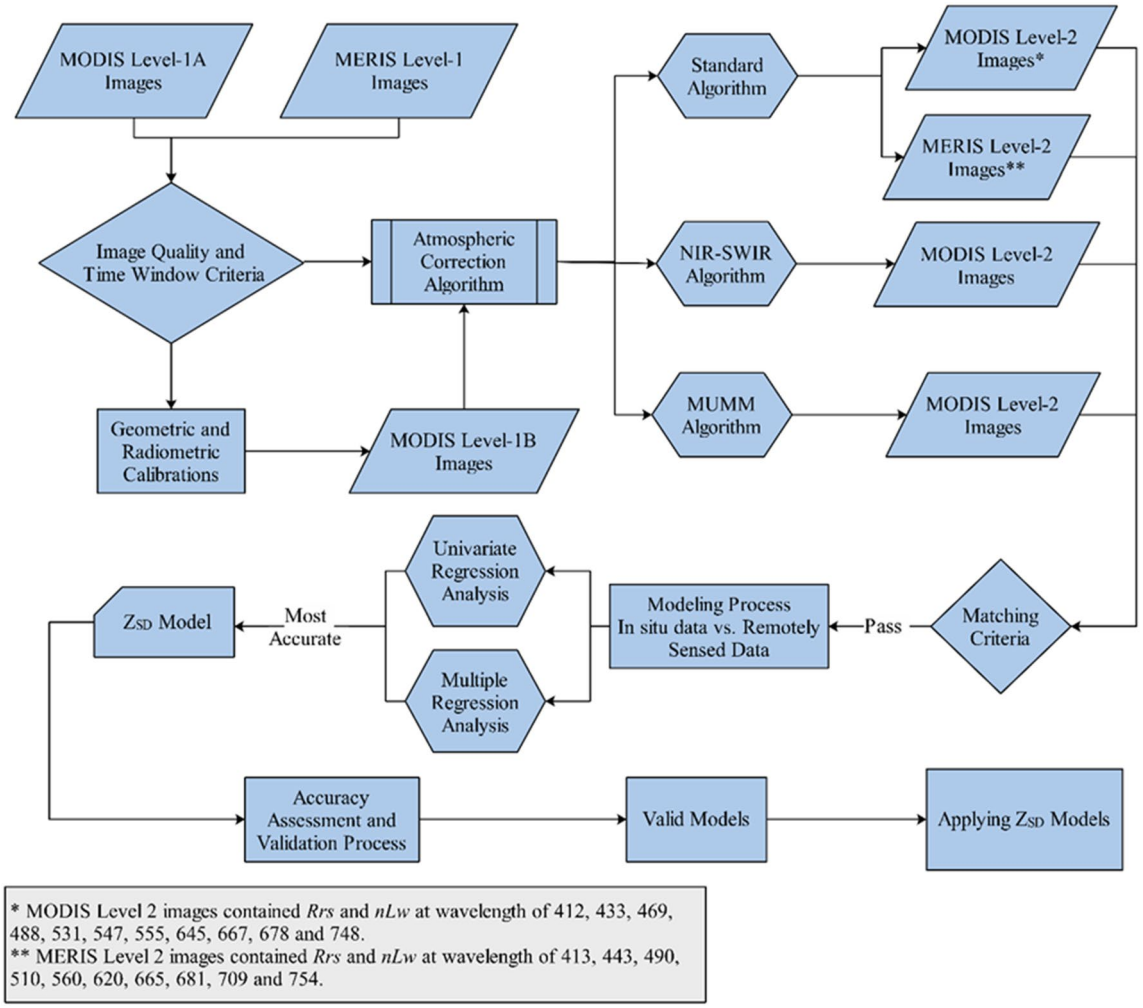

Fig. 2 An overview of methodology used to model Z_{SD}

n is the number of pixels within ($\pm 1.5 \times \sigma$) from the mean. Filtered means with n less than five were excluded.

The level-2 MODIS and MERIS data were further divided into different datasets based on four aggregation measures (M-30, M-15, median and filtered mean). These datasets were independently analyzed to find the most optimum aggregation measure for matching remotely sensed datasets with in situ Z_{SD}.

4.3 Modeling Z_{SD}

Modeling Z_{SD} went through three stages, i.e., preparation of variables, construction of Z_{SD} models, and accuracy assessment of models. As an initial step of constructing the Z_{SD} models, the normality of all variables (i.e., in situ Z_{SD}, Rrs and nLw derived from MODIS and MERIS level-2 images) was tested. Different types of transformations were applied on variables that were not normally distributed to improve the data distribution shape and linearity between the regressed variables of Z_{SD} models (Mertler and Reinhart 2016). Several Z_{SD} models were developed by regressing Rrs and nLw at wavelength extending from 413 to 754 nm on in situ Z_{SD} measurements; the MODIS and MERIS datasets were analyzed separately. The statistical relationship between in situ Z_{SD} and these spectral bands was investigated using univariate and multiple regression analyses (based on stepwise technique) to find the best model explaining the most Z_{SD} variations within NAG waters.

The accuracy of Z_{SD} models was evaluated using cross-validation techniques. The robustness of MODIS derived Z_{SD} models was assessed using 3–1 cross-validation. The dataset was divided into three segments; two segments were selected to build the model, and the third segment was used to validate the model accuracy. This procedure was repeated three times by rotating the segment role (Camstra and Boomsma 1992; Jonathan et al. 2000; D'Alimonte and Zibordi 2003). For MERIS-derived Z_{SD} models, the robustness of models was evaluated using the leave-one-out cross-validation (LOOCV) method due to the limited number of observations. In the LOOCV method, one observation from the dataset was used as a training sample, while the rest were used to construct the Z_{SD} model. This procedure was repeated until each observation was trained by switching the role of observations in each run. Cawley and Talbot (2004) stated that LOOCV provides an accurate estimation of the model robustness. The average root mean squared error (RMSE) derived from cross-validation analysis and coefficient of determination (r^2) were used

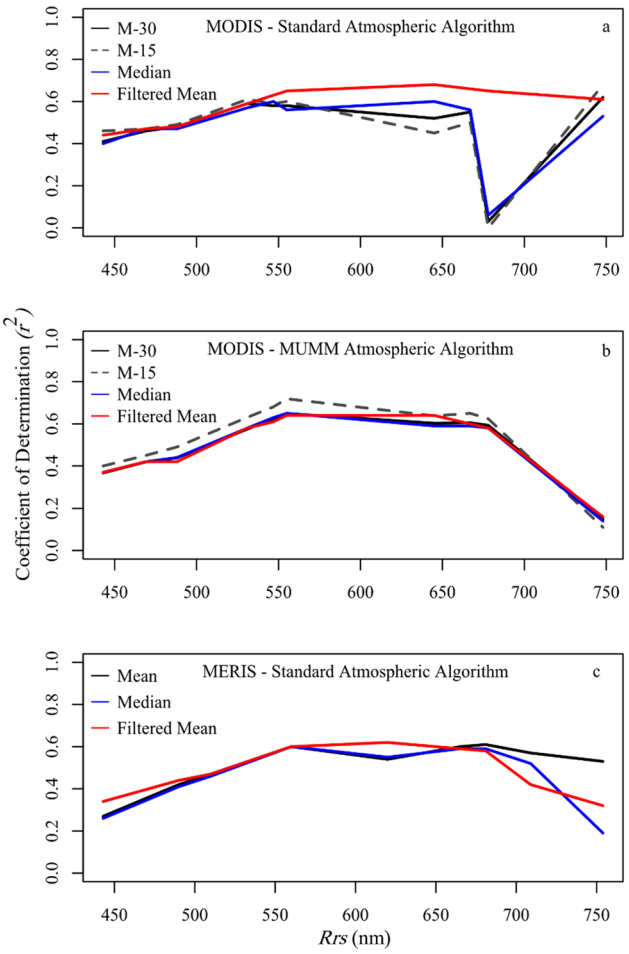

Fig. 3 **a** The MODIS $Rrs_{443to531}$ of the four datasets had a similar relationship with in situ Z_{SD}: Differences were clear beyond Rrs_{531} with an exception at Rrs_{678}. **b** The MODIS Rrs of the four datasets exhibited a similar relationship with in situ Z_{SD}. In general, Rrs dataset extracted using M-15 had the most significant relationship with in situ Z_{SD}. **c** The MERIS Rrs of the three datasets exhibited some variations in the relationship with in situ Z_{SD}. These variations were clear beyond Rrs_{681}

Table1 Coefficients of determination (r^2) between log-transformed in situ Z_{SD} and log-transformed MODIS Rrs atmospherically corrected using the standard algorithm

Rrs (λ)	M-30	M-15	Median	Filtered mean
443	0.41	0.46	0.4	0.44
469	0.46	0.47	0.47	0.47
488	0.48	0.49	0.47	0.48
531	**0.59**	**0.61**	**0.57**	**0.59**
547	**0.58**	**0.59**	**0.6**	**0.63**
555	**0.58**	**0.6**	**0.56**	**0.65**
645	**0.52**	0.45	**0.6**	**0.68**
667	**0.55**	**0.5**	**0.56**	**0.66**
678	0.03	0	0.06	0.65
748	**0.62**	**0.68**	**0.53**	**0.61**
n	144	111	152	151

The Rrs significantly explained the in situ Z_{SD} variations are bold. The Rrs_{412} was excluded from the analysis because it had a large amount of invalid values

Table 2 Coefficients of determination (r^2) between log-transformed in situ Z_{SD} and log-transformed MODIS Rrs atmospherically corrected using MUMM algorithm

Rrs (λ)	M-30	M-15	Median	Filtered mean
443	0.37	0.40	0.37	0.37
469	0.42	0.45	0.42	0.42
488	0.44	0.49	0.44	0.42
531	**0.58**	**0.63**	**0.58**	**0.58**
547	**0.63**	**0.68**	**0.63**	**0.61**
555	**0.65**	**0.72**	**0.65**	**0.64**
645	**0.60**	**0.64**	**0.59**	**0.64**
667	**0.61**	**0.65**	**0.59**	**0.6**
678	**0.59**	**0.62**	**0.58**	**0.58**
748	0.15	0.11	0.14	0.16
n	152	129	152	130

The Rrs significantly explained the in situ Z_{SD} variations are bold

Table 3 Coefficients of determination (r^2) between log-transformed in situ Z_{SD} and log-transformed MERIS Rrs

Rrs (λ)	Mean	Median	Filtered mean
443	0.27	0.26	0.34
490	0.42	0.41	0.44
510	0.47	0.46	0.47
560	**0.60**	**0.60**	**0.60**
620	**0.54**	**0.55**	**0.62**
665	**0.60**	**0.59**	**0.59**
681	**0.61**	**0.59**	**0.58**
709	**0.57**	**0.52**	0.42
754	**0.53**	0.19	0.32
n	72	72	72

The in situ Z_{SD} variations significantly explained by Rrs are bold

to sort the Z_{SD} models based on their robustness. The statistical analysis was carried out using R statistical programming language. Figure 2 illustrates an overview of methods used to model Z_{SD}.

5 Results

5.1 Simple Regression Analysis

In situ Z_{SD} observations were matched with Rrs and nLw products of MODIS and MERIS by calculating four aggregation measures (i.e., M-30, M-15, median and filtered mean) of 3 × 3 pixels centered at each corresponding in situ observation, meaning that the Rrs and nLw data were divided into four datasets based on these aggregation measures. Because the exclusion criteria of pixels values were different for each aggregation measure, the number of matching in situ observations corresponding to the aggregated pixel values varied. The Rrs and nLw products almost had the same relationship with in situ Z_{SD} observations. Thus, we reported the results of Rrs here for the sake of brevity. Also, the MODIS level-2 data estimated using the NIR-SWIR atmospheric correction algorithm were excluded at an early stage of the analysis due to the many invalid pixels yielded from using this algorithm. The NIR-SWIR atmospheric correction algorithm was clearly inefficient over the NAG compared to the Standard and MUMM algorithms.

The MODIS products of $Rrs_{531to645}$ atmospherically corrected using the standard algorithm had a significant general relationship with in situ Z_{SD} (Table 1), with an exception observed at Rrs_{645} extracted by M-15 ($r^2 = 0.45$). Contrarily, Rrs_{645} extracted using the filtered mean had the most significant relationship with in situ Z_{SD}. All Rrs datasets (i.e., those extracted by the different aggregation measures) exhibited, in general, a similar relationship with in situ Z_{SD} with two apparent exceptions at Rrs_{645} and Rrs_{678} (Fig. 3a). Among the four aggregation measures, the filtered mean returned a consistent relationship between Rrs and in situ Z_{SD}.

Furthermore, the MODIS products of $Rrs_{531to678}$ atmospherically corrected using MUMM algorithm exhibited a more consistent and significant relationship with in situ Z_{SD} than those estimated using the standard atmospheric correction algorithm (Table 2). The Rrs of the four datasets exhibited a generally consistent and similar relationship with in situ Z_{SD}. The Rrs_{555} had the most significant relationship with in situ Z_{SD}, especially the Rrs_{555} extracted by M-15 ($r^2 = 0.72$) (Fig. 3b). For the Rrs dataset extracted by the filtered mean, the most significant relationship with in situ Z_{SD} was observed at Rrs_{555} and Rrs_{645}($r^2 = 0.64$).

For the MERIS Rrs products, three datasets of $Rrs_{443to754}$ were extracted using mean, filtered mean and median of 3 × 3 pixels centered at each corresponding in situ observations, whereas excluding Rrs mean values based on their CV was not applied due to the limited number of matching points ($n = 72$). The $Rrs_{560to681}$ of the three datasets had a significant relationship with in situ Z_{SD} (Table 3). The most significant relationship between in situ Z_{SD} and MERIS Rrs was observed at Rrs_{620} extracted by the filtered mean ($r^2 = 0.62$). For the three datasets, $Rrs_{510and560}$ showed a similar relationship with in situ, whereas the relationship beyond Rrs_{681} varied among the three datasets (Fig. 3c).

5.2 Multiple Regression Analysis

Simple regression analysis revealed that Rrs (from MODIS and MERIS) responded differently to in situ Z_{SD} variations. The MODIS and MERIS Rrs at the green and red wavelengths ($\lambda > 530$ nm) were very responsive to in situ Z_{SD} variations, whereas the blue wavelengths were less responsive.

The red-edge and NIR wavelengths (700 nm < λ > 800 nm) exhibited an inconsistent relationship with in situ Z_{SD}. We observed that each spectral band from Rrs_{443} to Rrs_{754} explained an amount of in situ Z_{SD} variations that can be statistically incorporated in a single model using multiple regression analysis. Thus, we investigated all these bands together as predictors for in situ Z_{SD} to find those that most portray in situ Z_{SD} variations.

The MODIS level-2 products atmospherically corrected using the standard algorithm showed that the maximum variations of in situ Z_{SD} were explained by Rrs_{488} and Rrs_{748} extracted by M-15 ($R^2 = 0.73$). The Rrs extracted by M-30 and median responded differently to in situ Z_{SD} variations; Rrs_{678} and Rrs_{748} extracted by M-30 explained the most in situ Z_{SD} variations ($R^2 = 0.65$), whereas Rrs_{547} and Rrs_{645} extracted by the median value had the most significant relationship with in situ Z_{SD} ($R^2 = 0.64$) (Table 4). Multiple regression models using Rrs extracted by the filtered mean could not be established as they did not pass the analysis assumptions.

The MODIS Rrs estimated based on the MUMM atmospheric correction algorithm showed more consistent responses to in situ Z_{SD} variations than the Rrs estimated based on the standard atmospheric correction algorithm. The Rrs extracted by M-30 and median revealed that Rrs_{488} and Rrs_{555} explained the most in situ Z_{SD} variations ($R^2 = 0.75$ and $R^2 = 0.74$, respectively) (Table 4). The other Rrs datasets (i.e., those extracted by M-15 and filtered mean) did not pass the multiple regression analysis assumptions.

Table 4 Multiple regression models explained more in situ Z_{SD} variations than simple regression models

Regression analysis	Standard algorithm			MUMM algorithm	
	M-30	M-15	Median	M-30	Median
n	114	48	152	153	152
R^2	0.65	0.74	0.65	0.75	0.74
Adjusted R^2	0.64	0.73	0.64	0.75	0.74
Significance	0.00	0.00	0.00	0.00	0.00
b_0	0.659	− 1.34	0.777	0.522	0.489
b_1	− 0.589	− 0.975	− 0.536	− 2.53	− 2.449
b_2	0.079	5.242	− 0.234	1.482	1.383
Predictor 1	Rrs_{748}	Rrs_{748}	Rrs_{547}	Rrs_{555}	Rrs_{555}
Predictor 2	Rrs_{678}	Rrs_{488}	Rrs_{645}	Rrs_{488}	Rrs_{488}
RMSE	89 cm	270 cm	101 cm	80 cm	88 cm
Cross-validation RMSE	111 cm	295 cm	106 cm	85 cm	94 cm

The MUMM algorithm improved the efficiency of Rrs in estimating Z_{SD} · The Rrs_{555} and Rrs_{488} extracted M-30 were the most significant Z_{SD} predictors. Notice that the logarithmic transformation was applied to all Rrs and in situ Z_{SD} to improve the normality and linearity of these variables

Also, incorporating MERIS Rrs using multiple regression analysis to estimate Z_{SD} yielded a significant relationship; the Rrs_{681} and Rrs_{443} extracted by the mean value had the most significant relationship with in situ Z_{SD} variations ($R^2 = 0.78$). This relationship was changed ($R^2 = 0.66$) when extracting Rrs_{681} and Rrs_{443} using median. By extracting the Rrs using the filtered mean, the most significant predictors were different, i.e., Rrs_{620} and Rrs_{709} ($R^2 = 0.72$) (Table 5).

5.3 ZSD Model Accuracy Assessment

Significant MODIS Z_{SD} models derived through simple and multiple regression analyses (r^2 and $R^2 \geq 0.5$) were evaluated for accuracy and robustness using 3–1 cross-validation. The RMSEs of Z_{SD} models estimated by the cross-validation technique varied from 220 to 85 cm. Among the MODIS Z_{SD} models, the most accurate and robust model was the multiple regression model of Rrs_{555} and Rrs_{488} calculated using MUMM algorithm and extracted by M-30 (Table 4) (Fig. 4a, b). A demonstration of applying this model on MODIS level-2 data is illustrated in Fig. 5a; the model is mathematically expressed as:

$$Z_{SD}(\text{cm}) = 10^{0.522 - 2.53 \times \log Rrs_{555} + 1.482 \times \log Rrs_{488}} \quad (2)$$

Furthermore, MERIS models derived from simple and multiple regression analysis were evaluated for accuracy and robustness using the LOOCV technique. The RMSEs of MERIS models estimated by LOOCV technique varied from 84 to 74 cm showing robustness comparable to MODIS models derived from both atmospheric algorithms (Table 5). The most accurate and robustness Z_{SD} model was the multiple regression model of Rrs_{681} and Rrs_{443} (Fig. 4c, d). A demonstration of applying this model on MERIS level-2

Table 5 Statistical comparison between different modeling techniques using MERIS dataset

Regression analysis	Mean	Median	Filtered mean
n	72	72	64
R^2	0.78	0.66	0.72
Adjusted R^2	0.78	0.65	0.72
Significance	0.00	0.00	0.00
b_0	− 20.917	0.106	− 36.133
b_1	− 13.524	− 0.795	− 19.801
b_2	33.201	3.144	138.082
Predictor 1	log Rrs_{681}	log Rrs_{681}	log Rrs_{620}
Predictor 2	$\sqrt{Rrs_{433}}$	$\sqrt{Rrs_{433}}$	$\sqrt{Rrs_{709}}$
RMSE	74 cm	78 cm	79 cm
Cross-validation RMSE	77 cm	82 cm	82 cm

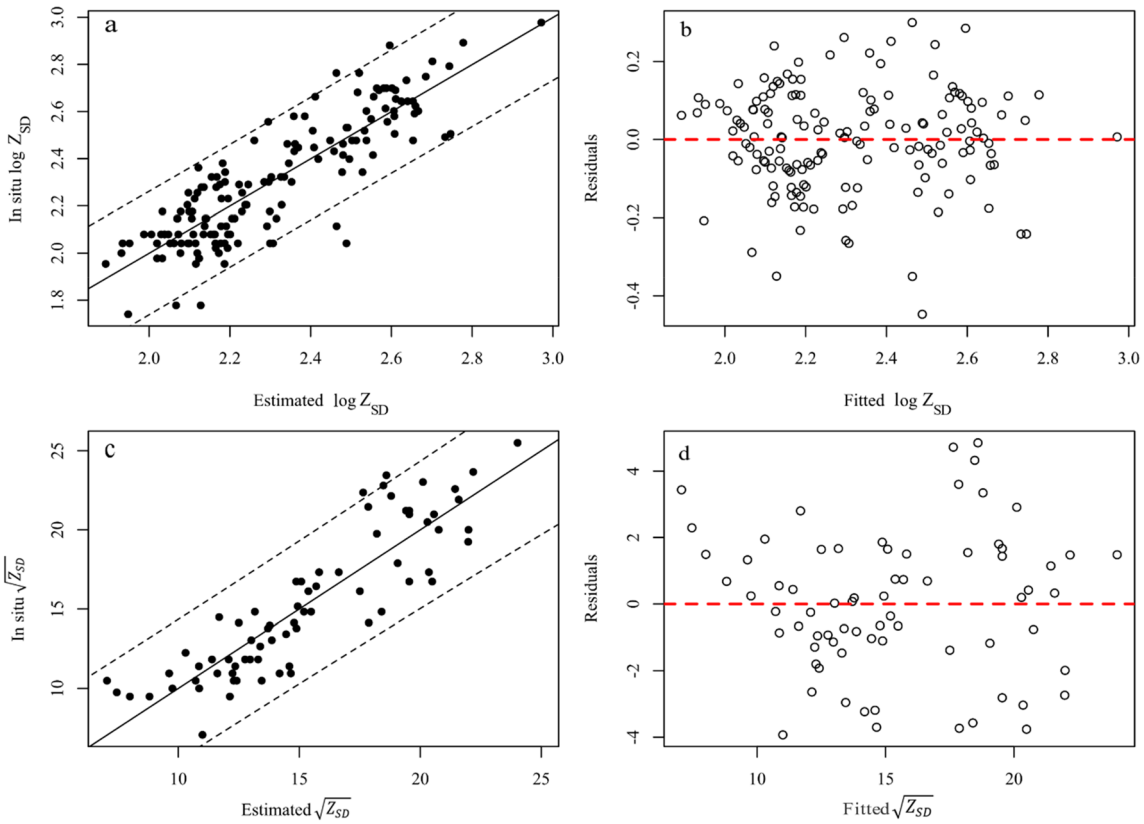

Fig. 4 **a** A scatter plot between actual and estimated log Z_{SD} values from the MODIS model. The area between the dotted lines in **a** and **c** is the prediction margin ($\alpha = 0.95$) that illustrates the model performance. For MODIS model (**b**) and MERIS model (**d**). the random pattern between residuals and fitted values shows the model's robustness, i.e., errors do not covary with Z_{SD} values. **c** A scatter plot between actual and estimated $\sqrt{Z_{SD}}$ values (denoted as $\sqrt{\text{insitu}Z_{SD}}$) from MERIS model

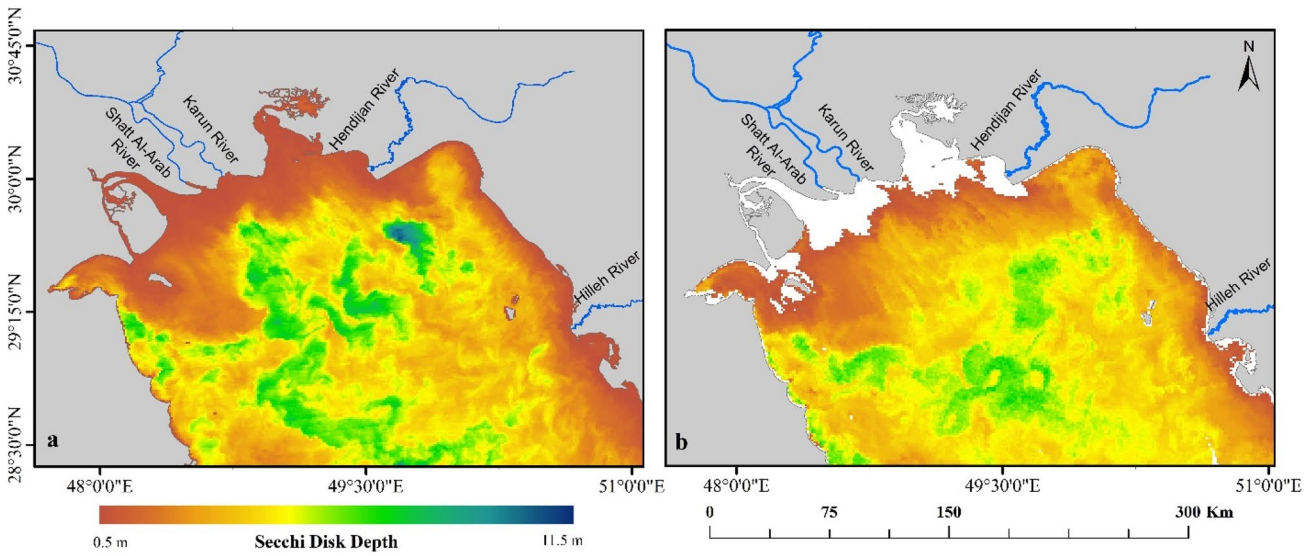

Fig. 5 **a** The MODIS Z_{SD} model applied on MODIS level-2 acquired in 3 Jan 2011. **b** The MERIS Z_{SD} model on MERIS level-2 acquired in 23 Jan 2011

data is illustrated in Fig. 5; the model is mathematically expressed as:

$$Z_{SD}(\text{cm}) = \left[-20.917 - \left(13.524 \times \log \text{Rrs}_{681}\right) + \left(33.201 \times \sqrt{\text{Rrs443}}\right)\right]^2 \quad (3)$$

6 Discussion

Modeling Z_{SD} using high temporal resolution satellite images, such as MODIS and MERIS, is essential for building synoptic water quality monitoring programs. In this study, two empirical Z_{SD} models were developed for NAG waters derived from MODIS and MERIS level-2 data. In developing the Z_{SD} models, we investigated the performance of three atmospheric correction algorithms (i.e., standard, NIR-SWIR and MUMM) over NAG waters and the suitability of four aggregation measures for extracting pixels (i.e., M-30, M-15, median and filtered mean). The consistent relationship between Z_{SD} and Rrs calculated using MUMM algorithm demonstrates the performance of this atmospheric correction algorithm over NAG waters. We observed that whatever the aggregation measure used to extract Rrs, the spectral responses to Z_{SD} variations had a uniform shape (Fig. 3b). Also, the standard atmospheric correction algorithm performed well when modeling Z_{SD} using MERIS level-2 data. Two possible explanations of this performance are the high spatial resolution that could reduce the heterogeneity of pixels matched with in situ data, and the use of a long wavelength (i.e., red) band that is less affected by atmospheric scattering factors (Goyens et al. 2013).

Furthermore, the comparison among the aggregation measures revealed that different pixel extraction criteria could yield different results. For instance, excluding the mean of heterogeneous pixels, whose CV ≥ 30%, improved the model's accuracy more than using the mean after excluding the outliers (i.e., the filtered mean), especially when the number of concurrent in situ observations with satellite data is relatively large ($n > 100$) (Mertler and Reinhart 2016). Using the filtered mean suggested by Bailey and Werdell (2006) to remedy the heterogeneity issue of matched pixels can be a practical alternative aggregation measure when the number of matching in situ observations is relatively small. Another suitable alternative aggregation measure is the median of pixels that was a good representative value of Rrs, whereas excluding the mean of pixels whose CV ≥ 15% was impractical because it reduced the number of candidate in situ observations.

The MODIS and MERIS Rrs at the visible spectrum were very responsive to in situ Z_{SD} variations. The Rrs at green bands had a high correlation with in situ Z_{SD} observations. Modeling Z_{SD} using the most responsive Rrs, however, was not the most optimum means to capture the maximum Z_{SD} variations as water transparency fluctuates by different water constituents that independently contribute to Rrs at different visible bands. For instance, CDOM significantly contributes to Rrs at blue and green regions, whereas TSS contributes to Rrs at red regions (Hu et al. 2004). Using the band ratioing approach to overcome this issue might not be the best solution. Considering that each spectral band contributes to explaining Z_{SD} differently, this approach does not efficiently control the contribution weight of bands being ratioed. Developing Z_{SD} models using multiple regression analysis can solve this issue through coefficients (slopes) that precisely determine the contribution of each predictor (Rrs) in explaining Z_{SD} variations (Mertler and Reinhart 2016). Using multiple regression is a straightforward and accurate approach to model OAPs when they have (directly or by transformation) a linear relationship with Rrs. In contrast, complicated nonlinear relationships between OAPs and Rrs can be efficiently modeled using neural network analysis (Zhang et al. 2002; Chen et al. 2015, 2019; Heddam 2016a). Yuan et al. (2017) and Chang et al. (2000), however, stated that the efficiency of neural network model varies with the training dataset selection, meaning that applying the model to data that differ from the training dataset might yield unreliable results.

Moreover, the uncertainties associated with Z_{SD} models can be induced by in situ Z_{SD} measurements that are influenced by multiple factors, such as the observer's visual acuity and water surface roughness (Preisendorfer 1986; Heddam 2016b; Alikas and Kratzer 2017). Visual acuity differences among observers would contribute to in situ Z_{SD} variations not related to the light intensity within the water column. Also, differences in water surface roughness due to boat movements and wind speed variations can be a source of error. These factors are intrusive during in situ Z_{SD} data collection and cannot be avoided. Thus, Z_{SD} models with an RMSE of about 75 cm seem to be very accurate considering these factors.

The proposed Z_{SD} models in this study improve the estimation of water transparency over NAG waters compared to the previous models of the Arabian Gulf region. Alsahli (2009) model ($r^2 = 0.68$), developed to estimate water transparency over Kuwait waters using MODIS level-2 data, and Al-Kaabi et al. (2016) model ($r^2 = 0.62$), developed to estimate water transparency over the Arabian Gulf region using MODIS level-2 data, had less performance than the proposed Z_{SD} MODIS in his study ($R^2 = 0.75$). The other factors that give more reality to the proposed Z_{SD} over the previous two models are the number of observations used to construct the models and the narrow matching time window. The previous two models were developed using observations ($n < 67$) less than what was used on the proposed Z_{SD} model ($n = 152$). Al-Kaabi et al. (2016) used a wider time window (± 6 h) to match satellite images with in situ observations

that might also not capture the temporal variability of Z_{SD} as they were insufficiently distributed over the months of the year.

Furthermore, the two previous models used the standard atmospheric correction algorithm and light attenuation coefficient at 488 nm (Kd_{488}) semi-analytically derived using Lee et al. (2005) model. The semi-analytical approach showed less performance than the empirical approach used in this study. Lee et al. (2015) proposed an improved approach of the previous semi-analytical model that performed well in estimating Z_{SD} in different places (Shang et al. 2016; Kulshreshtha and Shanmugam 2017). The performance of the current semi-analytical model, however, is questionable in highly turbid waters, especially those below 2 m as illustrated by Liu et al. (2019). Thus, using the empirical approach to model Z_{SD} of highly turbid waters where a large area of the water body has Z_{SD} below 2 m, such as NAG waters, is still the most favorable option.

The NAG ecosystems are significantly influenced by multiple local and regional factors, including extensive anthropogenic activities and high turbid fresh waters discharging from the rivers that carry a large amount of organic matters and nutrients from agricultural areas and other sources (Rahmanpour et al. 2014; Al-Mahmood and Mahmood 2019; Cunningham et al. 2019). These factors can disturb the NAG ecosystems in different ways. For instance, increasing organic matters induced by anthropogenic activities provides optimum conditions for heterotrophic plankton communities to grow and overgraze phytoplankton species leading to an imbalance status in the aquatic ecosystem by changing water quality indicators (e.g., dissolved oxygen, nitrogen, ammonium, and Chl-*a* concentrations) (Johannessen et al. 2006; Boufeniza et al. 2020). Thus, monitoring Z_{SD} over NAG waters in a synoptic perspective using ocean color satellite products can be significantly linked to biotic and abiotic activities. Monitoring these activities provides an early alert for catastrophic events and assists in controlling many polluting sources contributing to degrading NAG ecosystems. The MODIS and MERIS Z_{SD} models proposed in this study can be applied in water quality monitoring programs to significantly estimate water transparency of NAG and understand factors degrading its ecosystems (Alsahli and Nazeer 2021). Using the two models also can be extended to cover the entire Arabian Gulf, and probably similar waters, with some training data for the accuracy estimation.

7 Conclusion

Multiple regression analysis was performed to develop two empirical Z_{SD} models for NAG waters using MODIS and MERIS level-2 data. In constructing these two Z_{SD} models, the performance of three atmospheric correction algorithms (i.e., standard, NIR-SWIR and MUMM) over NAG waters and suitability of four aggregation measures used to extract Rrs (i.e., M-30, M-15, median and filtered mean) were evaluated. Among the three atmospheric correction algorithms, MUMM was the most suitable algorithm for the NAG. The comparison among the pixel extraction methods revealed that excluding severe heterogeneous groups of pixels, whose CV ≥ 30%, was the most appropriate extraction method. In contrast, using filtered mean might be an alternative extraction method when the number of matching in situ observations is relatively small.

The in situ Z_{SD} variations were significantly explained by the Z_{SD} models derived from the MODIS and MERIS level-2 Rrs products ($R^2 = 0.75$ and RSME = 80 cm, $R^2 = 0.78$ and RMSE = 74 cm, respectively). The uncertainties associated with Z_{SD} models can be induced by in situ Z_{SD} measurements that are influenced by multiple factors, such as the observer's visual acuity and water surface roughness. With this margin of error, however, the proposed Z_{SD} models improved the estimation of water transparency over NAG waters compared to the previous models of the Arabian Gulf region. The Z_{SD} models can be used to accurately map spatial and temporal distributions of Z_{SD} for NAG waters that would provide a better understanding of NAG water quality dynamics. Also, the two Z_{SD} models can be applied for the entire Arabian Gulf waters and probably other similar waters, with the availability of training data.

Acknowledgements The authors would like to thank the NASA Goddard Space Flight Center's Ocean Biology Processing Group for providing the MODIS Aqua products, the Kuwait Environmental Public Authority (KEPA), and Kuwait's Ministry of Public Works (MPW) for providing the in situ datasets. This research was funded by Kuwait University, Research Grant No. [RO02/16].

Funding This research was funded by Kuwait University, Research Grant No. [RO02/16].

Availability of Data and Materials Due to the nature of this research, participants of this study did not agree for their data to be shared publicly, so supporting data is not available.

Code Availability Inapplicable.

Declarations

Conflict of interest The authors declare that they have no known conflict of interests that could have appeared to influence the work reported in this paper.

References

Abuzinada AH, Barth H-J, Krupp F, Böer B, Al-Abdessalaam TZ (2008) Protecting the Gulf's marine ecosystems from pollution. Birkhauser

Al-Ghadban AN, El-Sammak A (2005) Sources, distribution and composition of the suspended sediments, Kuwait Bay, Northern Arabian Gulf. J Arid Environ 60:647–661. https://doi.org/10.1016/J.JARIDENV.2004.07.017

Alikas K, Kratzer S (2017) Improved retrieval of Secchi depth for optically-complex waters using remote sensing data. Ecol Ind. https://doi.org/10.1016/j.ecolind.2017.02.007

Al-Mahmood HK, Mahmood AB (2019) Effect of Karun River on the salinity status in the Shatt Al-Arab River, Basrah-Iraq. Mesopot J Mar Sci 34:13–26

Alsahli MM (2009) Characterizing surface temperature and clarity of Kuwait's seawaters using remotely sensed measurements and GIS analyses. University of Kansas

Alsahli MMM, Nazeer M (2021) Spatiotemporal variability of secchi depths of the North Arabian Gulf over the last two decades. Estuar Coast Shelf Sci 260:107487. https://doi.org/10.1016/J.ECSS.2021.107487

Al-Yamani F, Bishop J, Ramadhan E, Al-Husaini M, Al-Ghadban AN (2004) Oceanographic Atlas of Kuwait's Waters. Kuwait Insitute for Scientific Research

Bailey SW, Werdell PJ (2006) A multi-sensor approach for the on-orbit validation of ocean color satellite data products. Remote Sens Environ 102:12–23. https://doi.org/10.1016/J.RSE.2006.01.015

Boufeniza RL, Alsahli MM, Bachari NI, Bachari FH (2020) Spatiotemporal quantification and distribution of diatoms and dinoflagellates associated with algal blooms and human activities in Algiers Bay (Algeria) using Landsat-8 satellite imagery. Reg Stud Mar Sci. https://doi.org/10.1016/j.rsma.2020.101311

Camstra A, Boomsma A (1992) Cross-validation in regression and covariance structure analysis. Sociol Methods Res 21:89–115. https://doi.org/10.1177/0049124192021001004

Cawley GC, Talbot NLC (2004) Fast exact leave-one-out cross-validation of sparse least-squares support vector machines. Neural Netw 17:1467–1475. https://doi.org/10.1016/j.neunet.2004.07.002

Chang NB, Xuan Z, Jeffrey Yang Y (2013) Exploring spatiotemporal patterns of phosphorus concentrations in a coastal bay with MODIS images and machine learning models. Remote Sens Environ. https://doi.org/10.1016/j.rse.2013.03.002

Chang L-M, Chen P-H, Abdelrazig Y (2000) Intelligent diagnosis on bridge painting defects using image processing techniques. In: Brebbia CA, Samartin A (eds) Computational methods for smart structures and materials II. WIT Press, pp 1–10. https://doi.org/10.2495/SM000091

Chen Z, Muller-Karger FE, Hu C (2007) Remote sensing of water clarity in Tampa Bay. Remote Sens Environ 109:249–259. https://doi.org/10.1016/J.RSE.2007.01.002

Chen J, Yin S, Xiao R, Xu Q, Lin C (2014a) Deriving remote sensing reflectance from turbid Case II waters using green-shortwave infrared bands based model. Adv Space Res 53:1229–1238. https://doi.org/10.1016/J.ASR.2014.01.014

Chen S, Zhang T, Hu L (2014b) Evaluation of the NIR-SWIR atmospheric correction algorithm for MODIS-Aqua over the Eastern China Seas. Int J Remote Sens 35:4239–4251. https://doi.org/10.1080/01431161.2014.916051

Chen J, Zhu Y, Wu Y, Cui T, Ishizaka J, Ju Y (2015) A neural network model for $K(\lambda)$ retrieval and application to global Kpar monitoring. PLoS ONE 10:1–26. https://doi.org/10.1371/journal.pone.0127514

Chen J, Han Q, Chen Y, Li Y (2019) A Secchi depth algorithm considering the residual error in satellite remote sensing reflectance data. Remote Sens. https://doi.org/10.3390/rs11161948

Cherukuru N, Brando VE, Schroeder T, Clementson LA, Dekker AG (2014) Influence of river discharge and ocean currents on coastal optical properties. Cont Shelf Res. https://doi.org/10.1016/j.csr.2014.04.022

Constantin S, Doxaran D, Constantinescu S (2016) Estimation of water turbidity and analysis of its spatio-temporal variability in the Danube River plume (Black Sea) using MODIS satellite data. Cont Shelf Res. https://doi.org/10.1016/j.csr.2015.11.009

Cunningham PA, Sullivan EE, Everett KH, Kovach SS, Rajan A, Barber MC (2019) Assessment of metal contamination in Arabian/Persian Gulf fish: a review. Mar Pollut Bull. https://doi.org/10.1016/j.marpolbul.2019.04.007

D'Alimonte D, Zibordi G (2003) Phytoplankton determination in an optically complex coastal region using a multilayer perceptron neural network. IEEE Trans Geosci Remote Sens 41:2861–2868. https://doi.org/10.1109/TGRS.2003.817682

Delgado AL, Jamet C, Loisel H, Vantrepotte V, Perillo GME, Piccolo MC (2014) Evaluation of the MODIS-Aqua Sea-Surface Temperature product in the inner and mid-shelves of southwest Buenos Aires Province, Argentina. Int J Remote Sens 35:306–320. https://doi.org/10.1080/01431161.2013.870680

Doron M, Babin M, Hembise O, Mangin A, Garnesson P (2011) Ocean transparency from space: validation of algorithms estimating Secchi depth using MERIS, MODIS and SeaWiFS data. Remote Sens Environ 115:2986–3001. https://doi.org/10.1016/J.RSE.2011.05.019

European Space Agency (ESA) (2018) Sentinel-3 - Missions - Sentinel Online - Sentinel Online. https://sentinels.copernicus.eu/web/sentinel/missions/sentinel-3. Accessed 18 Nov

Franz BA, Kwiatowska EJ, Meister G, McClain CR (2008) Moderate resolution imaging spectroradiometer on Terra: limitations for ocean color applications. J Appl Remote Sens 2:023525. https://doi.org/10.1117/1.2957964

Goyens C, Jamet C, Schroeder T (2013) Evaluation of four atmospheric correction algorithms for MODIS-Aqua images over contrasted coastal waters. Remote Sens Environ 131:63–75. https://doi.org/10.1016/J.RSE.2012.12.006

Heddam S (2016a) Secchi disk depth estimation from water quality parameters: artificial neural network versus multiple linear regression models? Environ Process 3:525–536. https://doi.org/10.1007/s40710-016-0144-4

Heddam S (2016b) Secchi disk depth estimation from water quality parameters: artificial neural network versus multiple linear regression models? Environ Process. https://doi.org/10.1007/s40710-016-0144-4

Hu C, Carder KL, Muller-Karger FE (2000) Atmospheric correction of SeaWiFS imagery over turbid coastal waters: a practical method. Remote Sens Environ. https://doi.org/10.1016/S0034-4257(00)00080-8

Hu C, Chen Z, Clayton TD, Swarzenski P, Brock JC, Muller-Karger FE (2004) Assessment of estuarine water-quality indicators using MODIS medium-resolution bands: Initial results from Tampa Bay, FL. Remote Sens Environ 93:423–441. https://doi.org/10.1016/j.rse.2004.08.007

Johannessen T, Dahl E, Lindahl O (2006) Overgrazing of edible algae as a mechanism behind red tides and harmful algal blooms. Afr J Mar Sci. https://doi.org/10.2989/18142320609504173

Jonathan P, Krzanowski WJ, McCarthy WV (2000) On the use of cross-validation to assess performance in multivariate prediction. Stat Comput 10:209–229. https://doi.org/10.1023/A:1008987426876

Kaabi Al, Muna R, Zhao J, Ghedira H (2016) MODIS-based mapping of Secchi disk depth using a qualitative algorithm in the shallow Arabian Gulf. Remote Sens. https://doi.org/10.3390/rs8050423

Kaiser MJ, Attrill MJ, Jennings S, Thomas DN, Barnes DKA (2011) Marine ecology: processes, systems, and impacts, 2nd edn. Oxford University Press, New York

Karbassi AR, Nabi-Bidhendi GR, Bayati I (2005) Environmental geochemistry of heavy metals in a sediment core off Bushehr, Persian Gulf. Iran J Environ Health Sci Eng 2:255–260

Kulshreshtha A, Shanmugam P (2017) Estimation of underwater visibility in coastal and inland waters using remote sensing data. Environ Monit Assess. https://doi.org/10.1007/s10661-017-5905-7

Lee ZP, Darecki M, Carder KL, Davis CO, Stramski D, Joseph Rhea W (2005) Diffuse attenuation coefficient of downwelling irradiance: an evaluation of remote sensing methods. J Geophys Res C Oceans. https://doi.org/10.1029/2004JC002573

Lee Z, Shang S, Hu C, Du K, Weidemann A, Hou W, Lin J, Lin G (2015) Secchi disk depth: a new theory and mechanistic model for underwater visibility. Remote Sens Environ 169:139–149. https://doi.org/10.1016/J.RSE.2015.08.002

Lewis MR, Kuring N, Yentsch C (1988) Global patterns of ocean transparency: implications for the new production of the open ocean. J Geophys Res. https://doi.org/10.1029/jc093ic06p06847

Liu X, Lee Z, Zhang Y, Lin J, Shi K, Zhou Y, Qin B, Sun Z (2019) Remote sensing of secchi depth in highly turbid lake waters and its application with MERIS data. Remote Sens. https://doi.org/10.3390/rs11192226

Marzouni MB, Akhoundali AM, Moazed H, Jaafarzadeh N, Ahadian J, Hasoonizadeh H, Akhoondali A (2014) Evaluation of Karun River water quality scenarios using simulation model results. Int J Adv Biol Biomed Res 2:339–358

Mertler CA, Reinhart RV (2016) Advanced and multivariate statistical methods: practical application and interpretation, 6th edn. Routledge, New York

Nechad B, Ruddick KG, Park Y (2010) Calibration and validation of a generic multisensor algorithm for mapping of total suspended matter in turbid waters. Remote Sens Environ 114:854–866. https://doi.org/10.1016/J.RSE.2009.11.022

Nilson T, Rennel M, Luhamaa A, Hordo M, Olesk A, Lang M (2012) MERIS GPP/NPP product for Estonia: I. Algorithm and preliminary results of simulation. For Stud 56:56–78

Petus C, da Silva ET, Devlin M, Wenger AS, Álvarez-Romero JG (2014) Using MODIS data for mapping of water types within river plumes inthe Great Barrier Reef, Australia: towards the production of river plume risk maps for reef and seagrass ecosystems. J Environ Manag. https://doi.org/10.1016/j.jenvman.2013.11.050

Preisendorfer RW (1986) Secchi disk science: visual optics of natural waters. Limnol Oceanogr 31:909–926. https://doi.org/10.4319/lo.1986.31.5.0909

Rahmanpour S, Ghorghani NF, Ashtiyani SML (2014) Heavy metal in water and aquatic organisms from different intertidal ecosystems, Persian Gulf. Environ Monit Assess. https://doi.org/10.1007/s10661-014-3788-4

Ruddick KG, De Cauwer V, Park YJ, Moore G (2006) Seaborne measurements of near infrared water-leaving reflectance: the similarity spectrum for turbid waters. Limnol Oceanogr. https://doi.org/10.4319/lo.2006.51.2.1167

Seafarers SD, Lavender S, Beaugrand G, Outram N, Barlow N, Crotty D, Evans J, Kirby R (2017) Seafarer citizen scientist ocean transparency data as a resource for phytoplankton and climate research. PLoS ONE 12:e0186092

Shang S, Lee Z, Shi L, Lin G, Wei G, Li X (2016) Changes in water clarity of the Bohai Sea: observations from MODIS. Remote Sens Environ. https://doi.org/10.1016/j.rse.2016.08.020

Shi W, Wang M (2007) Detection of turbid waters and absorbing aerosols for the MODIS ocean color data processing. Remote Sens Environ. https://doi.org/10.1016/j.rse.2007.02.013

Shi Y, Zhang T, Tian L, Shi L (2014) Ocean transparency inversion and its merging from Terra-MODIS and NPP-VIIRS satellites on the Northwest Pacific. Int Geosci Remote Sens Symp. https://doi.org/10.1109/IGARSS.2014.6947455

Shi K, Zhang Y, Zhu G, Qin B, Pan D (2018) Deteriorating water clarity in shallow waters: evidence from long term MODIS and in-situ observations. Int J Appl Earth Obs Geoinf. https://doi.org/10.1016/j.jag.2017.12.015

Song KS, Li L, Tedesco L, Duan HT, Li LH, Du J (2014) Remote quantification of total suspended matter through empirical approaches for inland waters. J Environ Inf. https://doi.org/10.3808/jei.201400254

Stock A (2015) Satellite mapping of Baltic Sea Secchi depth with multiple regression models. Int J Appl Earth Obs Geoinf 40:55–64. https://doi.org/10.1016/J.JAG.2015.04.002

Toming K, Kutser T, Uiboupin R, Arikas A, Vahter K, Paavel B (2017) Mapping water quality parameters with Sentinel-3 ocean and land colour instrument imagery in the Baltic Sea. Remote Sens. https://doi.org/10.3390/rs9101070

Vaičiūtė D, Bresciani M, Bučas M (2012) Validation of MERIS bio-optical products with in situ data in the turbid Lithuanian Baltic Sea coastal waters. J Appl Remote Sens. https://doi.org/10.1117/1.jrs.6.063568

Wang M, Son SH, Shi W (2009) Evaluation of MODIS SWIR and NIR-SWIR atmospheric correction algorithms using SeaBASS data. Remote Sens Environ 113:635–644. https://doi.org/10.1016/J.RSE.2008.11.005

Wang M, Shi W, Jiang L (2012) Atmospheric correction using near-infrared bands for satellite ocean color data processing in the turbid western Pacific region. Opt Express. https://doi.org/10.1364/oe.20.000741

Yuan H, Yang G, Li C, Wang Y, Liu J, Yu H, Feng H, Xu B, Zhao X, Yang X (2017) Retrieving Soybean Leaf Area Index from unmanned aerial vehicle hyperspectral remote sensing: analysis of RF, ANN, and SVM regression models. Remote Sens 9:309. https://doi.org/10.3390/RS9040309

Zhang Y, Pulliainen J, Koponen S, Hallikainen M (2002) Application of an empirical neural network to surface water quality estimation in the Gulf of Finland using combined optical data and microwave data. Remote Sens Environ 81:327–336

Zhang Y, Liu X, Yin Y, Wang M, Qin B (2012) Predicting the light attenuation coefficient through Secchi disk depth and beam attenuation coefficient in a large, shallow, freshwater lake. Hydrobiologia 693:29–37. https://doi.org/10.1007/s10750-012-1084-2